Food and Bioprocess Technology
https://doi.org/10.1007/s11947-023-03218-7

RESEARCH

Application of FTIR Microspectroscopy in Oenology: Shedding Light on Cell Wall Composition of *Saccharomyces cerevisiae* Strains

Renato L. Binati[1] · Nicola Ferremi Leali[1] · Michele Avesani[1] · Elisa Salvetti[1] · Giovanna E. Felis[2] · Francesca Monti[3] · Sandra Torriani[1]

Received: 11 April 2023 / Accepted: 24 September 2023

Abstract
The evaluation of cell parietal components of yeasts is an important criterium for the selection of wine starters since they play a key role in the vinification process. The aim of this study was to characterize and compare the cell wall composition of four industrial (BM45, D47, EC1118, K1) and three native *Saccharomyces cerevisiae* (MY8, MY11, PEDRO2000E) wine strains by means of scanning and transmission electron microscopy and ATR-FTIR microspectroscopy. A statistically significant variability in the cell wall thickness and cell diameter was observed among the yeast cells, with native strains showing higher cell diameter values. FTIR microspectroscopy applied on the intact cells without any previous invasive treatment and on the separated cell walls highlighted profound differences among the strains in terms of the overall content of parietal polysaccharides as related to the thickness of the cell walls and in terms of the relative concentration of β-glucans and mannans in the cell walls. The strains EC1118, MY11, and PEDRO2000E showed a higher overall content of β-glucans and mannans, whose lower relative concentration in PEDRO2000E was compensated by a thicker cell wall; BM45 and D47 were characterized by a high relative concentration of polysaccharides in a thinner wall, while K1 and MY8 displayed a low relative concentration of polysaccharides. ATR-FTIR microspectroscopy allows identifying polysaccharide-rich yeast strains and can become a smart option for the selection of starter cultures to be used in oenology and for other applications in food industry, thanks to the interesting technological properties of parietal polysaccharides.

Keywords FTIR microspectroscopy · Electron microscopy · *Saccharomyces cerevisiae* · Wine yeasts · Cell wall · Parietal polysaccharides

Introduction

In winemaking, alcoholic fermentation is typically carried out by selected yeast strains belonging to the *Saccharomyces cerevisiae* species, thanks to its superior ability to overcome the stressful conditions encountered in a wine environment (Gonzalez & Morales, 2022). Specific criteria have been indicated to select *S. cerevisiae* starter cultures with suitable oenological properties. Beside basic features to assure the conversion of sugars into ethanol and CO_2, starters should provide desirable metabolites and aromatic compounds, without producing unpleasant flavors, and survive the biomass production dehydration process to obtain active dry yeasts (Matallana & Aranda, 2017). A myriad of *S. cerevisiae* strains is available, each presumably more suitable to a particular wine style, usually aiming to enhance wine quality and typical sensory traits (Bordet et al., 2021). Notwithstanding, the amplified competition in the wine market and the increased consumer demand for differentiated products require the development of well-characterized improved starters, aimed at meeting buying trends such as sparkling wines and wines with a low alcohol content (Loira et al., 2012). The fine-tuned screening of strains could take advantage of less-explored yeast features, such as the composition and properties of the cell wall (Domizio et al., 2017).

✉ Francesca Monti
francesca.monti@univr.it

[1] Department of Biotechnology, University of Verona, Strada Le Grazie 15, 37134 Verona, (VR), Italy

[2] VUCC-DBT, Verona University Culture Collection – Department of Biotechnology, University of Verona, Strada Le Grazie, 15, 37134 Verona, (VR), Italy

[3] Department of Computer Science, University of Verona, Strada Le Grazie 15, 37134 Verona, (VR), Italy

Published online: 10 October 2023

The cell wall is a polysaccharidic structure representing 15–25% of the cell dry weight; it is crucial to ensure *S. cerevisiae* stress tolerance properties and plays a role in many interactions with other cells and the surrounding environment (Alexandre & Guilloux-Benatier, 2006). Although its composition and functions change during the cell life cycle, it is mainly constituted by mannoproteins (25–50%) and β-linked glucans (60%; β-1,3, β-1,4, and β-1,6 glucans). β-1,4 glucans and β-1,6 glucans represent the minor portion of the total β-glucan content on cell walls, being side branches linked to the backbone of β-1,3 glucans (Kang et al., 2018; Ribéreau-Gayon et al., 2006). Chitin, constituted by β-1,4-linked N-acetyl-D-glucosamine residues, represents only 1–2% of the cell wall in *S. cerevisiae*. Glucans and chitins form the inner layer of the cell wall, in which the mannoproteins are embedded (Alexandre & Guilloux-Benatier, 2006; Kang et al., 2018).

Parietal polysaccharides are released by yeasts during alcoholic fermentation and during wine aging on lees after the end of fermentation, due to the autolysis of dead yeast cells. Both production and release of glycoproteins depend on the specific yeast strain and the nutritional conditions (Caridi, 2006; Snyman et al., 2021). The yeast autolytic process involves a triggered cascade of intracellular enzymatic hydrolysis to degrade cytoplasmic and cell wall components, resulting in their release into the wine matrix (Alexandre & Guilloux-Benatier, 2006).

Thanks to their molecular and structural configuration, yeast polysaccharides show interesting technological properties for the food and beverage industries (Vejarano, 2020). In winemaking, they contribute with protein, tannin, and tartrate stability to reduce haze formation and astringency; improve mouthfeel, aromatic complexity, and persistence; help stabilize color in red wines and foaming in sparkling wines; and remove ochratoxin A by adsorbing it (Domizio et al., 2017; Ortiz-Villeda et al., 2021). To enhance the content of mannoproteins, high mannoprotein-producing yeast starters with preferably rapid autolysis are selected for a greater release during wine fermentation and aging, or supplements based on inactivated yeast cells can be added during the process (Domizio et al., 2017; Vejarano, 2020).

Several studies addressed the autolysis of yeast cells and its impact on wine quality, mostly focussed on the molecules being released. Nevertheless, the differences in cell wall composition among yeast strains and the kinetics of biochemical modifications still need to be studied in more depth (Alexandre & Guilloux-Benatier, 2006; Burattini et al., 2008; Cavagna et al., 2010; Giovani et al., 2012). The cell ultrastructure and its structural changes during autolysis and other induced damages have been studied using electron microscopy techniques (Ferrario et al., 2014; Martínez-Rodríguez et al., 2001b; Peltzer et al., 2018). Another possible approach is based on the selective extraction of specific biomolecules to elucidate their characteristics. In this case, application of degradative techniques such as hydrolysis that can also be time-consuming is required. Furthermore, the analysis of cell monomers after hydrolysis, using spectrophotometric or chromatographic methods, is often limited to a single class of compounds (Liu et al., 2013; Moore et al., 2015; Snyman et al., 2021).

On the contrary, Fourier transform spectroscopy (FTIR) in the mid-infrared range is an accurate non-destructive technique that provides an overall evaluation of cell composition with minimum sample preparation, including information on functional groups or bonds in the biochemical components such as proteins, lipids, nucleic acids, and carbohydrates (Burattini et al., 2008).

In particular, infrared absorption in the attenuated total reflection (ATR) modality (ATR-FTIR), where a high refraction index crystal is put into contact with the samples resulting in a reduced photon beam penetration depth, represents a rapid technique, particularly sensitive to the cell wall components, that does not require neither infrared transparent supports nor previous invasive cell treatments (Alvarez-Ordóñez et al., 2011; Burattini et al., 2008). As such, it can be virtually applied to all the microorganisms that can be grown in culture (Lasch & Naumann, 2015).

In food and bioprocess research, the biochemical "fingerprints" obtained through infrared absorption spectroscopy in conjunction with multivariate statistical analysis have been used in various fields and for different applications: investigation on the microstructure and macroscopic rheological properties of food ingredients; detection of food toxins, spoilage, and adulteration; evaluation of impacts from thermal treatments; monitoring of fermentation processes and enzyme activity; study of antibiotic properties; control of biofilm formation; and differentiation and identification of diverse microbial species and strains (Lu et al., 2011; Wenning & Scherer, 2013; Hassoun et al., 2021; Fanari et al., 2022).

More specifically, regarding wine-related applications, besides yeast strains discrimination (Adt et al., 2010; Grangeteau et al., 2016; Moore et al., 2015; Oelofse et al., 2010), FTIR microspectroscopy was used to characterize biotechnological processes associated with cell modifications and growth-dependent phenomena, such as the main biochemical shifts induced by autolysis on *S. cerevisiae* cells (Burattini et al., 2008; Cavagna et al., 2010), physiological states of *S. cerevisiae* (exponential and stationary phase) during fermentation (Puxeu et al., 2015), biophysical stress responses of *Lachancea thermotolerans* to dehydration (Câmara et al., 2020), and biofilm formation capacity of the spoilage yeast *Brettanomyces bruxellensis* (Dimopoulou et al., 2021).

Nonetheless, the use of ATR-FTIR is still a relatively underexplored frontier in wine research, and to the best of

our knowledge, it has never been used in the screening of yeast strains based on their expected cell wall composition for specific technological applications.

The aim of this study was to characterize and compare the cell wall composition of four industrial (BM45, D47, EC1118, K1) and three native (MY8, MY11, PEDRO2000E) strains of *S. cerevisiae* by means of scanning and transmission electron microscopy and ATR-FTIR microspectroscopy coupled with multivariate statistical analysis and curve fitting. Since the concentration of parietal components can vary according to several conditions, such as growth phase, availability of nutrients, oxygen levels, temperature, and pH (Aguilar-Uscanga & François, 2003), an accurate standardization of the cultural conditions was implemented. The collected information may become an option for the successful selection of starters with interesting properties for the wine sector and, more generally, of polysaccharide-rich yeast strains in view of other various and different applications in food industry.

Material and Methods

Yeast Strains and Growth Conditions

The yeasts used in this study, their origin, and application are listed in Table 1. The four industrial strains of *S. cerevisiae* (BM45, D47, K1, and EC1118) were isolated from dry active yeasts and used as wet cultures. Particularly, the strain EC1118 was used as a reference, since its capacity to release mannoproteins has long been documented (Martínez-Rodríguez et al., 2001a). The three native strains of *S. cerevisiae* (MY8, MY11, and PEDRO2000E) were isolated from wine-producing regions in Italy and showed good fermentative performances; MY11 is a flocculent strain.

All yeasts were maintained under cryo-preservation at − 80 °C in the Verona University Culture Collection–Department of Biotechnology (VUCC-DBT).

To favor the accumulation of parietal mannoproteins and β-glucans in the strains of the dataset, yeast strains were cultured in YPD broth (10 g/L yeast extract, 20 g/L bacteriological peptone, 20 g/L dextrose) at 27 °C with 150 rpm shaking (Galichet et al., 2001). Kinetic growth of each yeast was monitored by measuring optical density (OD_{600}) every 2 h to harvest cultures in the early stationary phase for the subsequent analysis. From these cultures, cells were pelleted by centrifugation (3000 × *g*, 10 min, 4 °C) and then washed three times with physiological solution (0.9% w/v NaCl). All reagents were from Sigma-Aldrich (Milan, Italy), unless otherwise stated.

Electron Microscopy Study

For scanning electron microscopy (SEM) imaging, yeast cell pellets were fixed in 2% glutaraldehyde in phosphate buffer saline (PBS; pH 7.4) for 3 h at 4 °C. Then, samples were carefully washed with PBS. Post-fixation was performed for 1 h at 4 °C with OsO_4 (1%) (Serva Electrophoresis, Heidelberg, Germany) and FeCN (1.5%). Samples were dehydrated by incubation in increasingly concentrated acetone solutions. The cells were dried with CPD 030 critical point dryer (Bal-Tec, Balzers, Liechtenstein), metallized with MED 010 (Bal-Tec), and finally observed under the digital scanning microscope DSM 950 (Zeiss, Milan, Italy). Cell diameter was determined using the ImageJ software (National Institutes of Health, Bethesda, MD, https://imagej.net/ij/index.html), after acquiring 50 measurements for each yeast strain.

Preparation of yeast cells for transmission electron microscopy (TEM) followed the same first steps described above, up to the cell dehydration with acetone. Dehydrated samples were incubated at 60 °C for 20 min in several

Table 1 Collection of *Saccharomyces cerevisiae* strains used in this study and results of their characterization through electron microscopy. Cell wall thickness and cell diameter represented as the mean ± standard deviation of 50 replicates

Yeast strain	Origin	Application	Cell wall thickness (nm)	Cell diameter (µm)
BM45*	Brunello di Montalcino (Siena)	Red wines	125 ± 27^{d}	3.64 ± 0.73^{c}
D47*	Côtes du Rhône	White wines	133 ± 24^{cd}	3.73 ± 0.91^{bc}
EC1118*	Champagne	Sparkling wines	142 ± 28^{b}	3.39 ± 0.86^{c}
K1*	Languedoc	Icewine, Rosé and Red wines	147 ± 31^{b}	3.70 ± 0.88^{bc}
MY8	Valpolicella (Verona)	Amarone wine	141 ± 22^{bc}	4.28 ± 1.23^{b}
MY11	Valpolicella (Verona)	Amarone wine	n.d	n.d
PEDRO2000E	Valle dei Laghi (Trento)	Vino Santo Trentino	180 ± 23^{a}	5.27 ± 1.51^{a}

Different superscript letters in the same column indicate a significant difference in HSD Tukey test ($p < 0.05$)

n.d. not determined

*Lallemand Inc. (Castel d'Azzano, Italy)

changes of Epon-araldite resin and acetone solutions, in which the concentration of resin gradually increases to 100%. The cells, fixed and embedded in the resin, were placed in plastic molds containing liquid resin and polymerized overnight at 60 °C. Ultrathin sections of 70 nm were cut with an ultramicrotome Ultracut E (Reichert, Depew, USA), immersed in lead citrate solution, washed with deionized water, and observed with a Morgagni 268D electron microscope (FEI Company, Hillsboro, USA). Different age of the yeast cells or the region dissected by the diamond blade could bring variability in the measurements; hence, the thickness of the cell walls was determined by ImageJ using three measurements on 50 cells for each yeast strain.

Data of cell diameter and thickness of cell wall were compared by one-way ANOVA (analysis of variance), followed by the post hoc Tukey's HSD (honestly significant difference) test with a threshold for statistical significance of $p < 0.05$, using the package multcomp of R software version 4.1.2 (R Core Team, 2022).

Electron microscopy analyses were carried out at the Department of Neurosciences, Biomedicine and Movement Sciences (University of Verona).

Cell Wall Separation

Cell breakage and separation of cell walls from other cell components were obtained following the micro-method with glass beads described by Dallies et al. (1998). Briefly, cell pellets from 1 mL cultures were resuspended in 0.5 mL 10 mM Tris–HCl pH 8.0 in presence of 0.5 g of acid washed glass beads. Cells were lysed using a Mini-Beadbeater (Biospec Products, Bartlesville, USA), running four 1-min cycles at full speed, with 1-min intervals on ice. Breakage of at least 95% cells was verified by an optical microscope (Leica Microsystems, Buccinasco, Italy). The cell wall suspension was collected, while the glass beads were washed three times with cold Tris–HCl; then, the suspension and washing solution were pooled and centrifuged to obtain a cell wall pellet. This pellet was washed with deionized water and centrifuged again ($1300 \times g$, 10 min, 4 °C), until a clear supernatant was observed. The purity of the cell wall extracts was evaluated by analyzing the decrease in DNA concentration in the washing solutions at the end of the isolation protocol; the absorbance at 260 nm was measured by a BioPhotometer (Eppendorf, Milan, Italy).

The cell walls were immediately deposited on a steel slide for FTIR measurements.

ATR-FTIR Microspectroscopy

Steel slides were washed with ultrapure water and ethanol 70% v/v, before depositing, in duplicate, (i) the cells harvested in the stationary phase and (ii) the separated cell walls (see above section). A 10-µL spot of each cellular suspension was deposited on a steel slide. The slides were kept under ventilation at 40 °C for 24 h, to dry the droplets.

Mid-infrared spectra were acquired using a Vertex 70 Bruker Optics (Rosenheim, Germany) spectrometer coupled to a Hyperion 3000 vis/IR microscope equipped with a photoconductive MCT detector. Measurements were carried out in the 4000–700 cm^{-1} wavenumber range using a 100-µm diameter 20X Germanium ATR objective. Due to total reflection, the reduced photon beam penetration depth increases linearly from the highest wavenumbers to the lowest ones. In the present configuration, its estimated value is of the order of 0.2 nm in the high wavenumber range (towards 3000 cm^{-1}) up to 0.8 nm in the low wavenumber range (towards 900 cm^{-1}).

Five to ten point-by-point spectra were acquired for each sample with a spectral resolution of 4 cm^{-1} by co-adding 64 scans for each spectrum (27 s acquisition time). A typical single point spectrum is shown in Fig. 1.

Pre-treatment of the spectra was performed with the Opus 7.5 (Bruker Optics) software. Single-point spectra in the 1780–770 cm^{-1} range were converted from transmittance into absorbance and corrected for the baseline (using a rubber band type correction) as well as for the infrared beam penetration depth.

Representative average spectra of each strain were obtained by calculating the arithmetic mean. The average spectra were finally area normalized in the 1780–770 cm^{-1} range to allow comparison between the strains with respect to the same probed overall quantity of cell components.

Principal Component Analysis (PCA) was applied to the average spectra using the R software version 4.1.2 (R Core Team, 2022). A detailed analysis of the most meaningful absorption bands related to mannans, β-glucans, and chitins in the 1180–940 cm^{-1} range was done after peak identification through second derivative by means of a curve fitting procedure (Opus 7.5 software) based on the local least-squares method with Gaussian bands.

Results and Discussion

In this study, the cell wall composition of four industrial (BM45, D47, EC1118, K1) and three native (MY8, MY11, PEDRO2000E) strains of *S. cerevisiae* was characterized and compared by means of ATR-FTIR microspectroscopy. Comparison of ATR infrared spectra on the intact cells, even after area normalization, is not straightforward and required evaluating the effect of the cell wall thickness. In fact, the photon beam penetration depth due to total reflection was the same for all the strains and higher than the typical cell wall thickness. This means that ATR spectra acquired on the intact cells did not probe the entire cell but rather a cell

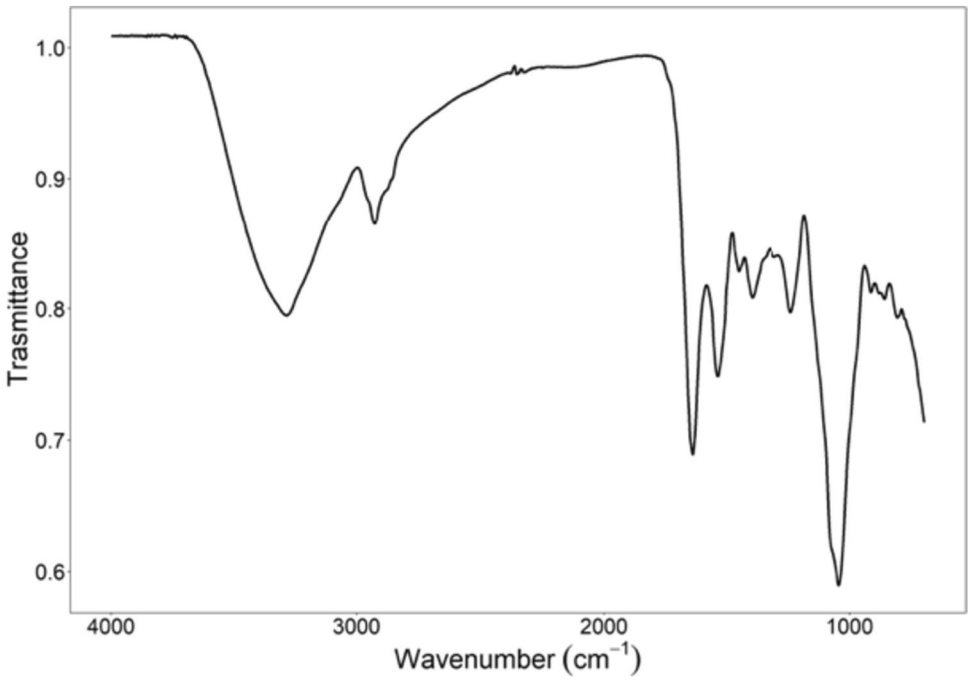

Fig. 1 Typical single-point ATR (attenuated total reflection) transmittance spectrum in the 4000–700 cm^{-1} range, acquired on the strain *Saccharomyces cerevisiae* PEDRO2000E

layer including the cell wall, the membrane, and part of the cytoplasm: a substantially different thickness of the cell wall determined the different contribution of the cytoplasm with respect to the cell wall in the area normalized spectra.

For a systematic analysis and understanding of FTIR spectra aimed at evaluating the relative content of oenologically relevant parietal polysaccharides in the seven strains, we measured the cell diameter and cell wall thickness of the strains through scanning and transmission electron microscopy.

Cellular Size and Cell Wall Ultrastructure

Electron microscopy analysis provided valuable information about the cellular size and ultrastructure of the studied *S. cerevisiae* strains. Figure 2 shows the cells of PEDRO2000E, while the SEM and TEM micrographs of the other yeasts are shown in Supplementary Fig. 1.

SEM method allowed acquisition of images of whole cells useful for quantification of average cellular size, while

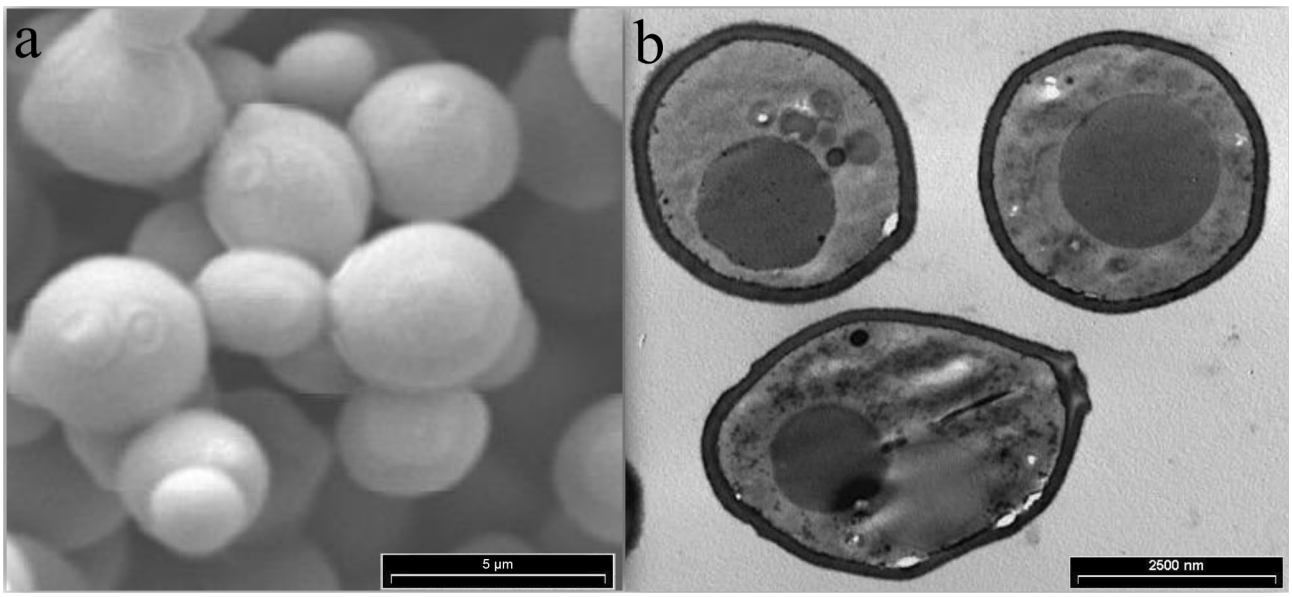

Fig. 2 Scanning electron microscopy (**a**) and transmission electron microscopy (**b**) images of cells of *Saccharomyces cerevisiae* PEDRO2000E

thin sections of cell (about 70 nm) observed under TEM allowed to estimate the cell wall thickness. MY11 was not included in the microscopic observations due to its peculiar characteristic of flocculation.

The estimated cell wall thickness and cell diameter of the *S. cerevisiae* strains are shown in Table 1. Cell diameter and cell wall thickness results obtained on EC1118 agree with those reported by Yamaguchi et al. (2011), who investigated the cell structure of *S. cerevisiae* strain S288c, a haploid derivative of EC1118, measuring an average diameter of 3.24 ± 0.42 µm and the cell wall was 120 ± 14 nm thick, thus, accordingly, slightly smaller and with a thinner wall compared with EC1118.

A certain variability in the ultrastructure among the six yeast cells was observed. The native strains PEDRO2000E and MY8 showed higher values of the cell diameter (5.27 ± 1.51 µm and 4.28 ± 1.23 µm, respectively) compared to the four commercial strains (from 3.39 ± 0.86 µm to 3.73 ± 0.91 µm).

Regarding the cell wall thickness, PEDRO2000E had the thickest wall (180 ± 23 nm) and BM45 and D47 the thinnest (125 ± 27 nm and 133 ± 24 nm, respectively), while EC1118, K1, and MY8 had intermediate values (from 141 ± 22 nm to 147 ± 31 nm). Since the IR beam penetration depth in ATR measurements can be estimated to be around 700–800 nm in the 1800–900 cm^{-1} range, this implies a lower contribution from the cell wall with respect to the cytoplasm in the spectra of BM45 and D47, and a higher contribution from the cell wall with respect to the cytoplasm in PEDRO2000E, and an intermediate situation for EC1118, K1, and MY8.

Infrared Spectra of the Cells: Band Assignments and Biochemical Composition

Figure 3 shows the average area normalized absorption spectra of the cells of the seven *S. cerevisiae* strains, which give information on the relative content of the various biochemical components of the cells. Since all the single-point spectra for the biological replicates of each strain gave reproducible results, the obtained average spectra are indeed representative of their behavior. Absorption bands were identified through second derivatives (Supplementary Fig. 2) and are reported in the Supplementary Table 1 together with their main assignments (Burattini et al., 2008; Cavagna et al., 2010; Hernández-Ramírez et al., 2021; Kumirska et al., 2010).

Visual inspection of the spectra showed interesting differences among the strains, with EC1118, MY11, and PEDRO2000E well distinguished from the other four strains. Moreover, it appears that the most meaningful absorption bands that better characterize and differentiate the samples in terms of both overall intensity and shape are in the 1180–900 cm^{-1} region. This agrees with the results obtained by Puxeu et al. (2015). These authors used multivariate statistical analysis of ATR-FTIR spectra to investigate three commercial *S. cerevisiae* strains during fermentation. All the absorption bands in this region are correlated to the yeasts' major parietal polysaccharides: mannans (mainly around 1045 cm^{-1} and 967 cm^{-1}) and β-glucans (β-1,3 mainly around 1132 cm^{-1} and 1105 cm^{-1}; β-1,4 around 1025 cm^{-1}; and β-1,6 around 995 cm^{-1}).

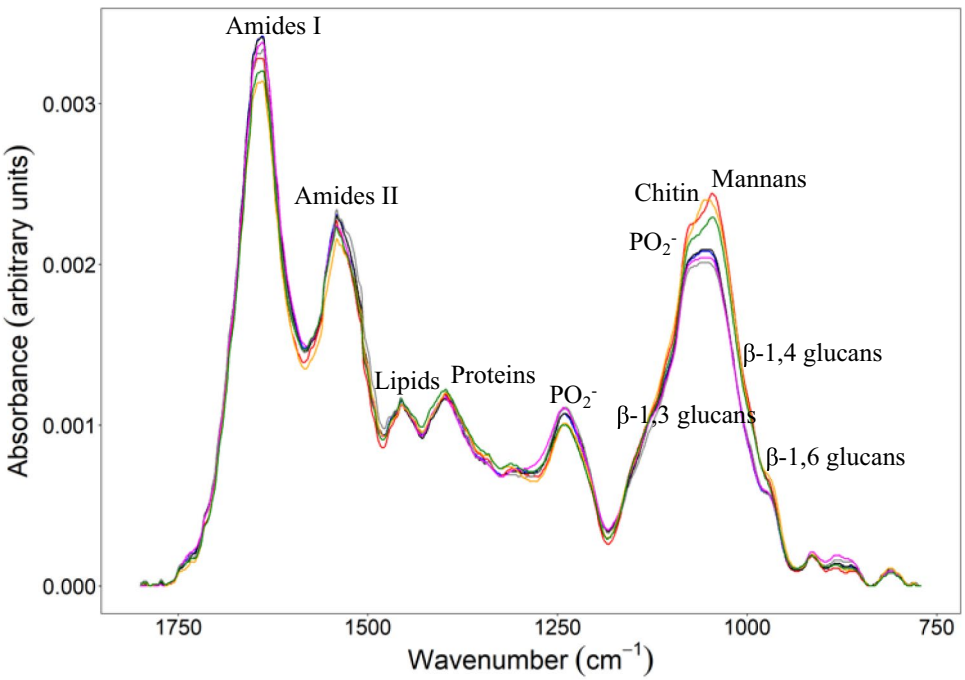

Fig. 3 Average area normalized ATR (attenuated total reflection) infrared absorbance spectra of cells of *Saccharomyces cerevisiae* strains: BM45 (blue line), D47 (gray), EC1118 (red), K1 (black), MY8 (fuchsia), MY11 (orange), and PEDRO2000E (green). Band assignments corresponding to the main biochemical components are also indicated

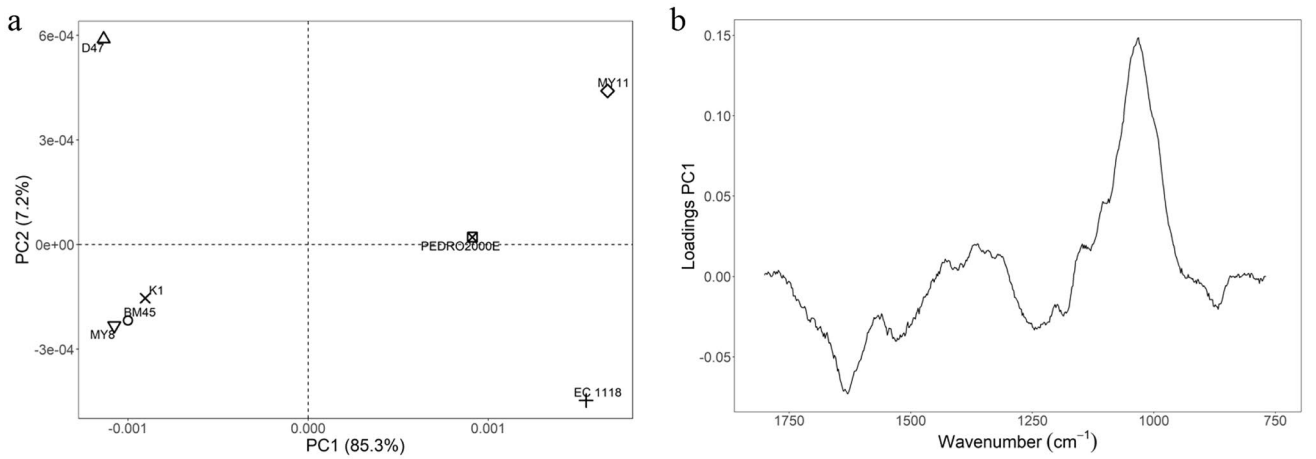

Fig. 4 PC1/PC2 (i.e., first/second principal component) score-score plot (**a**) and loadings on PC1 (**b**) from the Principal Component Analysis carried out in the 1800–700 cm^{-1} range on the averaged absorbance spectra of cells of *Saccharomyces cerevisiae* strains: BM45, D47, EC1118, K1, MY8, MY11, and PEDRO2000E

In particular, the absorption band at around 970 cm^{-1} can be correlated to the main glycosidic linkage of the mannans (Kato et al., 1973), while at 1045 cm^{-1}, a contribution from glycogen, present in the cell wall as well as in the cytoplasm, can also be acknowledged (Arvindekar & Patil, 2002; Kuligowski et al., 2012). Two other bands, at around 1154 cm^{-1} and 1060 cm^{-1}, can be confidently attributed to the less abundant chitin component (Cárdenas et al., 2004; Kumirska et al., 2010). Conversely, the band at around 1080 cm^{-1}, related to the phosphate group, although representing also the negatively charged phosphomannans found in the outer part of the cell wall, can be predominantly associated with nucleic acids in the cytoplasm and phospholipids of the membrane (Berterame et al., 2016; Hernández-Ramírez et al., 2021).

Principal Component Analysis (PCA) allowed for a statistically grounded grouping of the spectra while identifying the spectral components that mostly contribute to their discrimination (Fig. 4).

The PC1/PC2 score-score plot confirms that EC1118, MY11, and PEDRO2000E are well distinguished from the other four strains (Fig. 4a). The PC1 loadings indicate that this discrimination is due to the relatively higher intensity of the bands located in the 1180–900 cm^{-1} range (Fig. 4b). The differences among the spectra are better highlighted by the PCA done in the restricted 1180–900 cm^{-1} range (Fig. 5) without changing the normalization.

Discrimination between EC1118, PEDRO2000E, and MY11 on one side and BM45, D47, K1, and MY8 on the

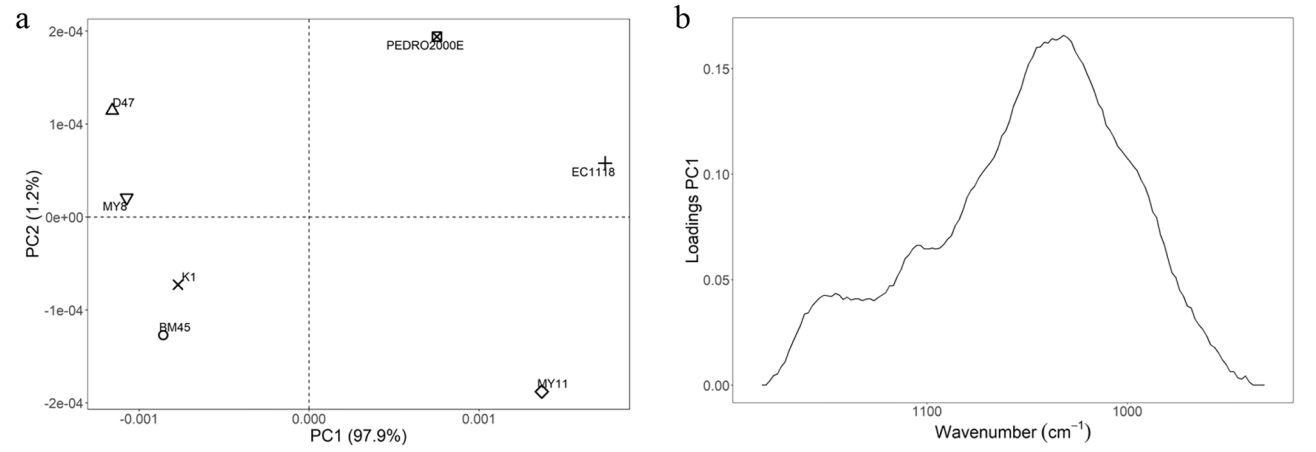

Fig. 5 PC1/PC2 (i.e., first/second principal component) score-score plot (**a**) and loadings on PC1 (**b**) from the Principal Component Analysis carried out in the 1180–900 cm^{-1} range on the averaged absorbance spectra of cells of *Saccharomyces cerevisiae* strains: BM45, D47, EC1118, K1, MY8, MY11, and PEDRO2000E

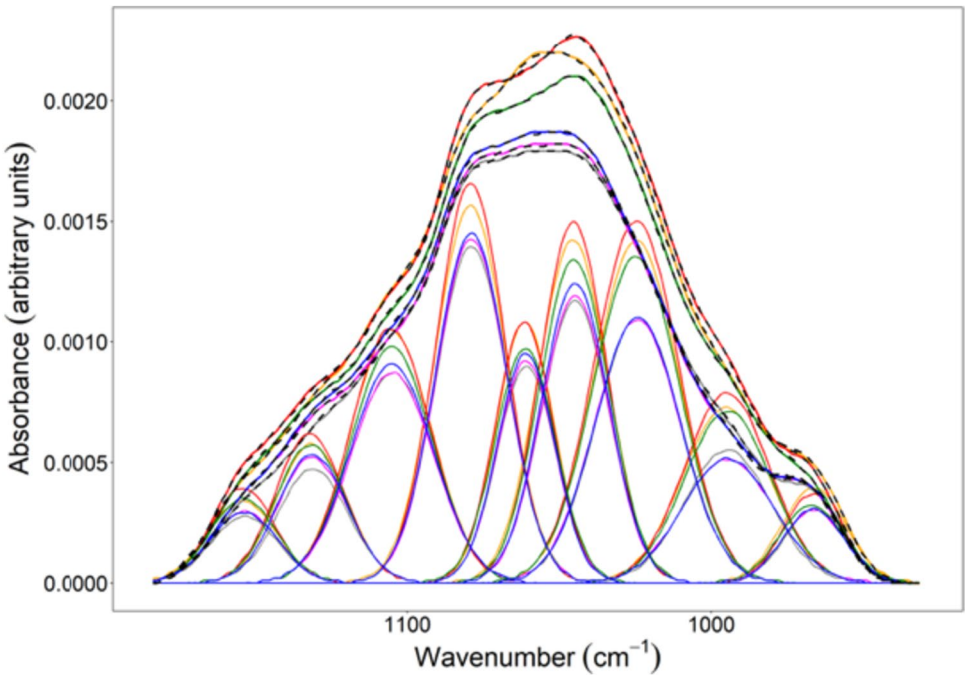

Fig. 6 Curve fitting (black dashed lines) results on the intact cell spectra of *Saccharomyces cerevisiae* strains BM45 (blue solid line), D47 (gray), EC1118 (red), MY8 (fuchsia), MY11 (orange), and PEDRO2000E (green). Spectrum and curve fitting results on the strain K1 cannot be visually distinguished from BM45 ones and are omitted from the figure for the sake of clarity

other is evident along the first principal component with a very high value of the captured variance (97.9%) and is mainly due to the absorption bands related to mannans (1045 cm^{-1}) and β-1,4 glucans (1025 cm^{-1}).

A more detailed investigation of the various contributions was obtained after curve fitting. Curve fitting was carried out with nine Gaussian bands and identified from the minima of the second derivatives of the spectra. Figure 6 shows the results of the fits, while band intensities together with their corresponding assignments (Burattini et al., 2008; Kumirska et al., 2010) are shown in Table 2.

As a whole, intensities of the bands in the 1180–940 cm^{-1} range are all higher in EC1118, PEDRO2000E, and MY11 than in the other four strains.

These results, relative to the total probed composition in the 1780–770 cm^{-1} range, depend on the interplay between the different relative concentration of the cell wall components and the different thickness of the cell walls in each strain and are affected by the presence of the phosphate band at 1080 cm^{-1} mainly related to intracellular nucleic acids and membrane phospholipids of each strain.

Infrared Spectra of the Separated Cell Walls: Comparison with the Intact Cells

To get an in-depth view of the cell wall composition of the strains, ATR-FTIR measurements were performed on the cell walls separated from the intracellular structures. Figure 7a

Table 2 Intensities of the absorption bands relative to the total probed composition (in %) after curve fitting in the 1180–940 cm^{-1} range on the average absorbance spectra of intact cells for the seven *Saccharomyces cerevisiae* strains

Peak (cm^{-1})	Main band assignments*	Strains						
		EC1118	MY11	PEDRO2000E	K1	BM45	MY8	D47
967	Mannans	0.9	1.0	0.8	0.8	0.8	0.8	0.8
995	β-1,6 glucans	2.8	2.6	2.6	2.0	1.9	1.9	2.0
1025	**β-1,4 glucans**	**5.2**	**4.9**	**4.8**	**3.9**	**3.8**	**3.8**	**3.9**
1045	**Mannans**	**4.1**	**4.1**	**3.8**	**3.4**	**3.4**	**3.3**	**3.3**
1061	Chitins	2.6	2.6	2.4	2.3	2.3	2.2	2.2
1079	PO_2^-	4.7	4.6	4.4	4.2	4.2	4.2	4.1
1105	β-1,3 glucans	3.5	3.5	3.3	3.1	3.1	3.0	3.0
1132	β-1,3 glucans	1.8	1.7	1.7	1.5	1.5	1.5	1.4
1154	Chitins	1.0	1.0	1.0	0.8	0.8	0.8	0.8

Asterisk (*) indicates that the main assignments are based on the literature (Burattini et al., 2008; Cavagna et al., 2010; Hernández-Ramírez et al., 2021; Kumirska et al., 2010). Bold numbers indicate the most distinctive bands among the different strains

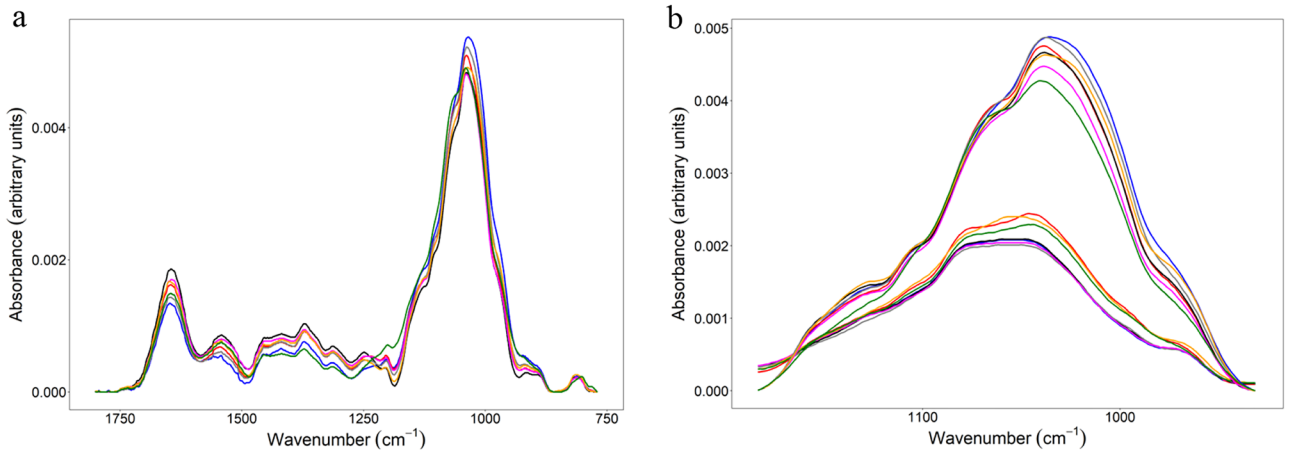

Fig. 7 Average area normalized absorption spectra of the separated cell walls of *Saccharomyces cerevisiae* strains (**a**) and the same spectra in the restricted 1180–940 cm^{-1} range compared to the intact cells (of lower intensity) with the same normalization (**b**): BM45 (blue line), D47 (gray), EC1118 (red), K1 (black), MY8 (fuchsia), MY11 (orange), and PEDRO2000E (green)

shows the average area normalized absorption spectra for the separated cell walls, which give information on the relative concentration of the various biochemical components in the cell walls. In Fig. 7b, the same spectra in the restricted 1180–940 cm^{-1} range are compared to the intact cells (always with the usual area normalization in the full 1780–770 cm^{-1} range). Second derivative data (Supplementary Fig. 2) confirmed that the phosphate 1080 cm^{-1} band, now related only to the mannosylphosphate moiety of the cell wall mannans, was strongly reduced. The presence of residual amide I, amide II, and other protein-related bonds can be attributed to cell wall mannoproteins (Peltzer et al., 2018). Moreover, elimination of the intracellular structures resulted in a substantial shifting towards higher wavenumbers of some of the other bands, especially of those related to β-1,6 glucans and chitins.

Figure 8 shows that the bands that mostly discriminate among the spectra (PC1 loadings, Fig. 8b) are due to β-glucans, mostly β-1,6 band, found at around 1008 cm^{-1}.

Interestingly, looking at the PC1 scores in the PC1/PC2 score-score plot (Fig. 8a), grouping of the spectra roughly reflects the same trends observed in the measurements of the cell wall thickness (Table 1). PEDRO2000E, which has the thickest wall, has a lower intensity of the β-1,6 glucan band, while BM45 and D47, which have the thinnest walls, have a higher intensity of the β-1,6 glucan band. K1, EC1118, and MY8, which showed intermediate cell wall widths, are in the middle. The relative band intensities after the curve fitting (Supplementary Fig. 3) confirmed these observations (Table 3).

The key differences between the results obtained for the intact cells and for the separated cell walls are highlighted

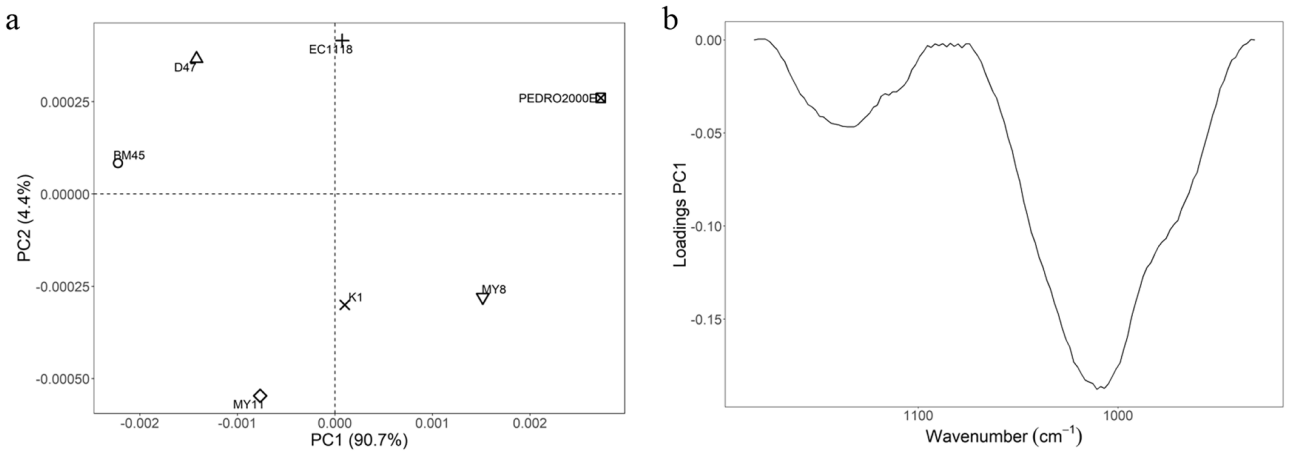

Fig. 8 PC1/PC2 (i.e., first/second principal component) score-score plot (**a**) and loadings on PC1 (**b**) from the Principal Component Analysis carried out in the 1180–900 cm^{-1} range on the averaged absorbance spectra of the separated cell walls of *Saccharomyces cerevisiae* strains BM45, D47, EC1118, K1, MY8, MY11, and PEDRO2000E

Table 3 Intensities of the absorption bands relative to the total probed composition (in %) after curve fitting in the 1180–940 cm^{-1} range on the average absorbance spectra of separated cell walls for the seven *Saccharomyces cerevisiae* strains

Peak (cm^{-1})	Main band assignments*	Strains						
		BM45	D47	MY11	EC1118	K1	MY8	PEDRO2000E
970	**Mannans**	**5.5**	**4.7**	**5.1**	**4.1**	**4.2**	**3.9**	**3.7**
1008	**β-1,6 glucans**	**13.9**	**13.4**	**12.8**	**12.2**	**12.2**	**11.1**	**10.4**
1028	β-1,4 glucans	6.5	6.5	6.1	6.4	6.2	6.0	5.6
1046	Mannans	10.3	10.2	10.0	10.1	9.9	9.8	9.7
1069	Chitins	7.7	7.9	7.7	8.0	7.6	7.6	7.8
1083	PO_2^-	1.9	2.0	2.0	1.9	1.9	1.9	2.0
1101	β-1,3 glucans	6.2	6.2	6.3	6.2	6.2	6.0	6.0
1131	**β-1,3 glucans**	**3.7**	**3.6**	**3.8**	**3.4**	**3.7**	**3.4**	**3.0**
1155	Chitins	1.9	2.0	2.0	2.0	2.0	1.9	1.6

Asterisk (*) indicates that the main assignments are based on the literature (Burattini et al., 2008; Cavagna et al., 2010; Hernández-Ramírez et al., 2021; Kumirska et al., 2010). Bold numbers indicate the most distinctive bands among the different strains

by PCA on all the average spectra after area normalization in the 1180–900 cm^{-1} range (Fig. 9).

Intact cells and separated cell walls are well distinguished (with 98% of the captured variance) by the first principal component (Fig. 9a). The corresponding loadings (Fig. 9b) confirm that the most discriminating bands were at 1080 cm^{-1} (PO_2^-), more intense in the intact cells, and at 1008 cm^{-1} (β-1,6 glucans), more intense in the separated cell walls.

Final Evaluation of the Content of Parietal Polysaccharides

The results obtained for the intact cells automatically consider the differences in the cell wall thickness and show that differentiation among the strains is mainly due to the content of mannans (absorption bands at 1045 cm^{-1}) and of β-1,4 glucans (absorption band at 1025 cm^{-1}). FTIR spectra acquired on the separated cell walls highlight the relative intensities of the absorption bands directly related to the concentration of the various biochemical components in the cell walls and allowed identifying and excluding contributions from the plasmatic membrane and from the cytoplasm, most notably due to PO_2^- groups at around 1080 cm^{-1}. In the case of the separated cell walls, differentiation among the strains is mainly due to the relative concentration of β-1,6 glucans, given by the intensities of the absorption bands found at around 1008 cm^{-1}. Interestingly, their behavior roughly reflects, in a reversed order, the same trend observed in the cell wall thickness.

Table 4 summarizes electron microscopy and infrared microspectroscopy outcomes giving a final synoptical comparison of the observed relative trends on the intact cells and cell walls of seven strains.

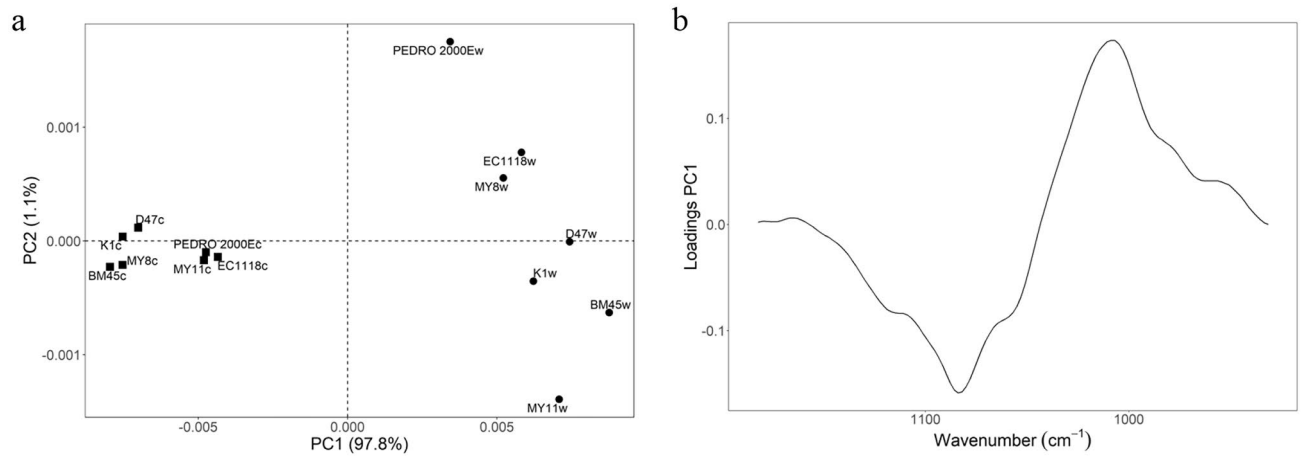

Fig. 9 PC1/PC2 (i.e., first/second principal component) score-score plot (**a**) and loadings on PC1 (**b**) from the Principal Component Analysis carried out on the absorption spectra, area normalized in the 1180–900 cm^{-1} range, of the intact cells (squares) and of the separated cell walls (dots) of *Saccharomyces cerevisiae* strains BM45, D47, EC1118, K1, MY8, MY11, and PEDRO2000E

Table 4 Summary of the results obtained with scanning and transmission electron microscopy and FTIR (Fourier transform infrared) microspectroscopy of intact cells and cell walls of the seven analyzed *Saccharomyces cerevisiae* strains

Characteristic	Strain						
	BM45	D47	EC1118	K1	MY8	MY11	PEDRO2000E
Cell diameter	↓	↓	↓	↓	↔	n.d	↑
Cell wall thickness	↓	↓	↔	↔	↔	n.d	↑
Relative concentration of polysaccharides in the cell wall	↑	↑	↔	↓	↓	↑	↓
Overall content of parietal polysaccharides in intact cells	↓	↓	↑	↓	↓	↑	↑

In each row, the upward, downward, and left–right arrows indicate higher, lower, and intermediate values for each strain as compared to the other strains

n.d. not determined

Altogether these results highlight profound differences among the *S. cerevisiae* strains analyzed. The cells of EC1118, MY11, and PEDRO2000E have the highest overall content of parietal polysaccharides. The lower relative concentration of β-glucans and mannans in the cell walls of PEDRO2000E as compared to EC1118 and MY11 is compensated by the thicker cell wall. Thus, these three strains showed the greatest potential in view of oenological applications, as active fermentation starters or yeast derivative products, for which a high release of polysaccharides is an important goal (Rigou et al., 2021; Snyman et al., 2021). Among the four strains with an overall low content of mannans and β-glucans, BM45 and D47, even though they showed a high relative concentration of polysaccharides in the cell walls, have a thinner wall, while K1 and MY8, with similar results to EC1118 regarding the wall thickness, had a lower relative concentration of polysaccharides. Comparing native with industrial strains, no significant differences were observed concerning the cell wall composition, although the native strains showed an overall higher cell diameter.

The difference in cell wall composition found for the wine *S. cerevisiae* strains analyzed in this study can be technologically exploited and extended to various kinds of applications in food industry: mannoproteins can be utilized for their high emulsifying and stabilizing properties and health-promoting benefits (Li & Karboune, 2018), while β-glucans, besides being a supplement in animal feed, have potent positive effects on the human immune system (Borchani et al., 2014). In addition, yeast strains rich in mannans and β-glucans can contribute to a more sustainable winemaking based on waste valorization strategies. In fact, the sediment formed at the bottom of tanks after the end of fermentation is mainly formed by dead yeast cells together with tartaric acid and grape marc. This winemaking residue can have a notable environmental impact if not properly managed. Bioactive compounds in the wine lees, such as polysaccharides, polyphenols, and organic acids, are becoming important targets for the recovery and exploitation of value-added products. Due to their interesting nutritional and technological properties, yeast parietal polysaccharides (mannoproteins and β-glucans) can justify investments in recycling technologies (De Iseppi et al., 2019; Mejia et al., 2022; Peltzer et al., 2018), since the use of polysaccharide-rich yeast strains could lead to a fraction of wine lees with increased valuable compounds.

Conclusions

This study confirmed that ATR-FTIR microspectroscopy in the mid-infrared represents a rapid, accurate, and sensitive method to characterize yeast cell wall composition. It is a powerful yet underexplored technique that can be directly applied to the cell cultures without previous invasive cell treatments and may become an option for the selection of yeast strains according to the properties of major interest for the wine sector, such as the content of parietal macromolecules and their eventual release. Application of ATR-FTIR spectroscopy on the separated cell walls and cell imaging through electron microscopy gave us important insights about the relative concentration of main compounds in the cell wall and about its correlation with the cell wall thickness, confirming the robustness of integrating direct ATR-FTIR measurements on the intact cells in a yeast selection program.

In perspective, some physico-chemical parameters that influence the content of parietal polymers could be investigated in the most promising strains to define optimal conditions for maximizing their accumulation, including trials with natural grape must under real winery conditions.

Supplementary Information The online version contains supplementary material available at https://doi.org/10.1007/s11947-023-03218-7.

Acknowledgements The authors thank Matteo Cavagna and Paolo Campostrini for technical assistance. The authors acknowledge the facilities and the staff scientific and technical assistance of the Department of Neurosciences, Biomedicine and Movement Sciences (University of Verona).

Author Contribution Conceptualization: R. L. B., F. M., and S. T.; methodology: F. M. and S. T.; formal analysis: R. L. B., N. F. L., and F. M.; investigation: R. L. B., N. F. L., M. A., and E. S.; resources: G. F., F. M., and S. T.; writing—original draft preparation: R. L. B., N. F. L., and M. A.; writing—review and editing: R. L. B., N. F. L., M. A., E. S., G. F., F. M., and S. T.; visualization and supervision: E. S., F. M., and S. T.; funding acquisition: F. M. and S. T.

Funding Open access funding provided by Università degli Studi di Verona within the CRUI-CARE Agreement. PhD scholarship of N.F.L. was funded by REACT-EU FSE in the frame of PON "Ricerca e Innovazione" 2014–2020 (DM 1061/2021). Codice BIO13, DOT1340225, Borsa 1 CUP B39J21026610001.

Data Availability The data presented in this study are available from the corresponding author on reasonable request.

Declarations

Conflict of Interest The authors declare no competing interests.

References

Adt, I., Kohler, A., Gognies, S., Budin, J., Sandt, C., Belarbi, A., Manfait, M., & Sockalingum, G. D. (2010). FTIR spectroscopic discrimination of *Saccharomyces cerevisiae* and *Saccharomyces bayanus* strains. *Canadian Journal of Microbiology, 56*, 793–801. https://doi.org/10.1139/w10-062

Aguilar-Uscanga, B., & François, J. M. (2003). A study of the yeast cell wall composition and structure in response to growth conditions and mode of cultivation. *Letters in Applied Microbiology, 37*, 268–274. https://doi.org/10.1046/j.1472-765x.2003.01394.x

Alexandre, H., & Guilloux-Benatier, M. (2006). Yeast autolysis in sparkling wine – A review. *Australian Journal of Grape and Wine Research, 12*, 119–127. https://doi.org/10.1111/j.1755-0238.2006.tb00051.x

Alvarez-Ordóñez, A., Mouwen, D. J., López, M., & Prieto, M. (2011). Fourier transform infrared spectroscopy as a tool to characterize molecular composition and stress response in foodborne pathogenic bacteria. *Journal of Microbiological Methods, 84*, 369–378. https://doi.org/10.1016/j.mimet.2011.01.009

Arvindekar, A. U., & Patil, N. B. (2002). Glycogen–A covalently linked component of the cell wall in Saccharomyces cerevisiae. *Yeast, 19*, 131–139. https://doi.org/10.1002/yea.802

Berterame, N. M., Porro, D., Ami, D., & Branduardi, P. (2016). Protein aggregation and membrane lipid modifications under lactic acid stress in wild type and OPI1 deleted *Saccharomyces cerevisiae* strains. *Microbial Cell Factories, 15*, 39. https://doi.org/10.1186/s12934-016-0438-2

Borchani, C., Fonteyn, F., Jamin, G., Paquot, M., Blecker, C., & Thonart, P. (2014). Enzymatic process for the fractionation of baker's yeast cell wall (*Saccharomyces cerevisiae*). *Food Chemistry, 163*, 108–113. https://doi.org/10.1016/j.foodchem.2014.04.086

Bordet, F., Roullier-Gall, C., Ballester, J., Vichi, S., Quintanilla-Casas, B., Gougeon, R. D., Julien-Ortiz, A., Kopplin, P. S., & Alexandre, H. (2021). Different wines from different yeasts? "*Saccharomyces cerevisiae* intraspecies differentiation by metabolomic signature and sensory patterns in wine". *Microorganisms, 9*, 2327. https://doi.org/10.3390/microorganisms9112327

Burattini, E., Cavagna, M., Dell'Anna, R., Malvezzi Campeggi, F., Monti, F., Rossi, F., & Torriani, S. (2008). A FTIR microspectroscopy study of autolysis in cells of the wine yeast *Saccharomyces cerevisiae*. *Vibrational Spectroscopy, 47*(2), 139–147. https://doi.org/10.1016/j.vibspec.2008.04.007

Câmara, A. A., Nguyen, T. D., Saurel, R., Sandt, C., Peltier, C., Dujourdy, L., & Husson, F. (2020). Biophysical stress responses of the yeast *Lachancea thermotolerans* during dehydration using synchrotron-FTIR microspectroscopy. *Frontiers in Microbiology, 11*, 899. https://doi.org/10.3389/fmicb.2020.00899

Cárdenas, G., Cabrera, G., Taboada, E., & Miranda, S. P. (2004). Chitin characterization by SEM, FTIR, XRD, and ^{13}C cross polarization/mass angle spinning NMR. *Journal of Applied Polymer Science, 93*, 1876–1885. https://doi.org/10.1002/app.20647

Caridi, A. (2006). Enological functions of parietal yeast mannoproteins. *Antonie Van Leeuwenhoek, 89*, 417–422. https://doi.org/10.1007/s10482-005-9050-x

Cavagna, M., Dell'Anna, R., Monti, F., Rossi, F., & Torriani, S. (2010). Use of ATR-FTIR microspectroscopy to monitor autolysis of *Saccharomyces cerevisiae* cells in a base wine. *Journal of Agricultural and Food Chemistry, 58*(1), 39–45. https://doi.org/10.1021/jf902369s

Dallies, N., François, J., & Paquet, V. (1998). A new method for quantitative determination of polysaccharides in the yeast cell wall. Application to the cell wall defective mutants of *Saccharomyces cerevisiae*. *Yeast, 14*, 1297–1306. https://doi.org/10.1002/(SICI)1097-0061(1998100)14:14%3c1297::AID-YEA310%3e3.0.CO;2-L

De Iseppi, A., Curioni, A., Marangon, M., Vincenzi, S., Kantureeva, G., & Lomolino, G. (2019). Characterization and emulsifying properties of extracts obtained by physical and enzymatic methods from an oenological yeast strain. *Journal of the Science of Food and Agriculture, 99*, 5702–5710. https://doi.org/10.1002/jsfa.9833

Dimopoulou, M., Kefalloniti, V., Tsakanikas, P., Papanikolaou, S., & Nychas, G. E. (2021). Assessing the biofilm formation capacity of the wine spoilage yeast *Brettanomyces bruxellensis* through FTIR spectroscopy. *Microorganisms, 9*, 587. https://doi.org/10.3390/microorganisms9030587

Domizio, P., Liu, Y., Bisson, L. F., & Barile, D. (2017). Cell wall polysaccharides released during the alcoholic fermentation by *Schizosaccharomyces pombe* and *S. japonicus*: Quantification and characterization. *Food Microbiology, 61*, 136–149. https://doi.org/10.1016/j.fm.2016.08.010

Fanari, F., Carboni, G., Desogus, F., Grosso, M., & Wilhelm, M. (2022). A chemometric approach to assess the rheological properties of durum wheat dough by indirect FTIR measurements. *Food and Bioprocess Technology, 15*, 1040–1054. https://doi.org/10.1007/s11947-022-02799-z

Ferrario, M., Guerrero, S., & Alzamora, S. M. (2014). Study of pulsed light-induced damage on *Saccharomyces cerevisiae* in apple juice by flow cytometry and transmission electron microscopy. *Food and Bioprocess Technology, 7*, 1001–1011. https://doi.org/10.1007/s11947-013-1121-9

Galichet, A., Sockalingum, G. D., Belarbi, A., & Manfait, M. (2001). FTIR spectroscopic analysis of *Saccharomyces cerevisiae* cell walls: Study of an anomalous strain exhibiting a pink-colored cell phenotype. *FEMS Microbiology Letters, 197*, 179–186. https://doi.org/10.1111/j.1574-6968.2001.tb10601.x

Giovani, G., Rosi, I., & Bertuccioli, M. (2012). Quantification and characterization of cell wall polysaccharides released by non-*Saccharomyces* yeast strains during alcoholic fermentation. *International Journal of Food Microbiology, 160*, 113–118. https://doi.org/10.1016/j.ijfoodmicro.2012.10.007

Gonzalez, R., & Morales, P. (2022). Truth in wine yeast. *Microbial Biotechnology, 15*, 1339–1356. https://doi.org/10.1111/1751-7915.13848

Grangeteau, C., Gerhards, D., Terrat, S., Dequiedt, S., Alexandre, H., Guilloux-Benatier, M., von Wallbrunn, C., & Rousseaux, S. (2016). FT-IR spectroscopy: A powerful tool for studying the inter- and intraspecific biodiversity of cultivable non-*Saccharomyces* yeasts isolated from grape must. *Journal of Microbiological Methods, 121*, 50–58. https://doi.org/10.1016/j.mimet.2015.12.009

Hassoun, A., Aït-Kaddour, A., Sahar, A., & Cozzolino, D. (2021). Monitoring thermal treatments applied to meat using traditional methods and spectroscopic techniques: A review of advances over the last decade. *Food and Bioprocess Technology, 14*, 195–208. https://doi.org/10.1007/s11947-020-02510-0

Hernández-Ramírez, J. O., Merino-Guzmán, R., Téllez-Isaías, G., Vázquez-Durán, A., & Méndez-Albores, A. (2021). Mitigation of AFB1-related toxic damage to the intestinal epithelium in broiler chickens consumed a yeast cell wall fraction. *Frontiers in Veterinary Science, 8*, 677965. https://doi.org/10.3389/fvets.2021.677965

Kang, X., Kirui, A., Muszyński, A., Widanage, M. C. D., Chen, A., Azadi, P., Wang, P., Mentink-Vigier, F., & Wang, T. (2018). Molecular architecture of fungal cell walls revealed by solid-state NMR. *Nature Communications, 9*, 2747. https://doi.org/10.1038/s41467-018-05199-0

Kato, K., Nitta, M., & Mizuno, T. (1973). Infrared spectroscopy of some mannans. *Agricultural and Biological Chemistry, 37*, 433–435. https://doi.org/10.1080/00021369.1973.10860687

Kuligowski, J., Quintás, G., Herwig, C., & Lendl, B. (2012). A rapid method for the differentiation of yeast cells grown under carbon and nitrogen-limited conditions by means of partial least squares discriminant analysis employing infrared micro-spectroscopic data of entire yeast cells. *Talanta, 99*, 566–573. https://doi.org/10.1016/j.talanta.2012.06.036

Kumirska, J., Czerwicka, M., Kaczyński, Z., Bychowska, A., Brzozowski, K., Thöming, J., & Stepnowski, P. (2010). Application of spectroscopic methods for structural analysis of chitin and chitosan. *Marine Drugs, 8*, 1567–1636. https://doi.org/10.3390/md8051567

Lasch, P., & Naumann, D. (2015). Infrared spectroscopy in microbiology. In Encyclopedia of Analytical Chemistry, R.A. Meyers (Ed.). https://doi.org/10.1002/9780470027318.a0117.pub2

Li, J., & Karboune, S. (2018). A comparative study for the isolation and characterization of mannoproteins from *Saccharomyces cerevisiae* yeast cell wall. *International Journal of Biological Macromolecules, 119*, 654–661. https://doi.org/10.1016/j.ijbiomac.2018.07.102

Liu, D., Lebovka, N. I., & Vorobiev, E. (2013). Impact of electric pulse treatment on selective extraction of intracellular compounds from *Saccharomyces cerevisiae* yeasts. *Food and Bioprocess Technology, 6*, 576–584. https://doi.org/10.1007/s11947-011-0703-7

Loira, I., Morata, A., González, C., & Suárez-Lepe, J. A. (2012). Selection of glycolytically inefficient yeasts for reducing the alcohol content of wines from hot regions. *Food and Bioprocess Technology, 5*, 2787–2796. https://doi.org/10.1007/s11947-011-0604-9

Lu, X., Al-Qadiri, H. M., Lin, M., & Rasco, B. A. (2011). Application of mid-infrared and Raman spectroscopy to the study of bacteria. *Food and Bioprocess Technology, 4*, 919–935. https://doi.org/10.1007/s11947-011-0516-8

Martínez-Rodríguez, A. J., Carrascosa, A. V., Barcenilla, J. M., Pozo-Bayón, M. Á., & Polo, M. C. (2001a). Autolytic capacity and foam analysis as additional criteria for the selection of yeast strains for sparkling wine production. *Food Microbiology, 18*, 183–191. https://doi.org/10.1006/fmic.2000.0390

Martínez-Rodríguez, A. J., Polo, M. C., & Carrascosa, A. V. (2001b). Structural and ultrastructural changes in yeast cells during autolysis in a model wine system and in sparkling wines. *International Journal of Food Microbiology, 71*, 45–51. https://doi.org/10.1016/s0168-1605(01)00554-2

Matallana, E., & Aranda, A. (2017). Biotechnological impact of stress response on wine yeast. *Letters in Applied Microbiology, 64*, 103–110. https://doi.org/10.1111/lam.12677

Mejia, J. A. A., Ricci, A., Figueiredo, A. S., Versari, A., Cassano, A., de Pinho, M. N., & Parpinello, G. P. (2022). Membrane-based operations for the fractionation of polyphenols and polysaccharides from winery sludges. *Food and Bioprocess Technology, 15*, 933–948. https://doi.org/10.1007/s11947-022-02795-3

Moore, J. P., Zhang, S. L., Nieuwoudt, H., Divol, B., Trygg, J., & Bauer, F. F. (2015). A multivariate approach using attenuated total reflectance mid-infrared spectroscopy to measure the surface mannoproteins and β-glucans of yeast cell walls during wine fermentations. *Journal of Agricultural and Food Chemistry, 63*, 10054–10063. https://doi.org/10.1021/acs.jafc.5b03154

Oelofse, A., Malherbe, S., Pretorius, I. S., & Du Toit, M. (2010). Preliminary evaluation of infrared spectroscopy for the differentiation of *Brettanomyces bruxellensis* strains isolated from red wines. *International Journal of Food Microbiology, 143*, 136–142. https://doi.org/10.1016/j.ijfoodmicro.2010.08.004

Ortiz-Villeda, B., Lobos, O., Aguilar-Zuniga, K., & Carrasco-Sánchez, V. (2021). Ochratoxins in wines: A review of their occurrence in the last decade, toxicity, and exposure risk in humans. *Toxins, 13*, 478. https://doi.org/10.3390/toxins13070478

Peltzer, M. A., Salvay, A. G., Delgado, J. F., de la Osa, O., & Wagner, J. R. (2018). Use of residual yeast cell wall for new biobased materials production: Effect of plasticization on film properties. *Food and Bioprocess Technology, 11*, 1995–2007. https://doi.org/10.1007/s11947-018-2156-8

Puxeu, M., Andorra, I., & De Lamo-Castellví, S. (2015). Monitoring *Saccharomyces cerevisiae* grape must fermentation process by attenuated total reflectance spectroscopy. *Food and Bioprocess Technology, 8*, 637–646. https://doi.org/10.1007/s11947-014-1435-2

R Core Team. (2022). R: A language and environment for statistical computing; R Foundation for Statistical Computing: Vienna, Austria. www.R-project.org/

Ribéreau-Gayon, P., Dubourdieu, D., Donèche, B., & Lonvaud, A. (2006). Cytology, taxonomy and ecology of grape and wine yeasts. Handbook of Enology, vol. 1. The microbiology of wine and vinifications, 2nd Edition, 1–51. John Wiley & Sons, West Sussex, England

Rigou, P., Mekoue, J., Sieczkowski, N., Doco, T., & Vernhet, A. (2021). Impact of industrial yeast derivative products on the modification of wine aroma compounds and sensorial profile. A Review. *Food Chemistry, 358*, 129760

Snyman, C., Mekoue Nguela, J., Sieczkowski, N., Marangon, M., & Divol, B. (2021). Optimised extraction and preliminary characterisation of mannoproteins from non-*Saccharomyces* wine yeasts. *Foods, 10*, 924. https://doi.org/10.3390/foods10050924

Vejarano, R. (2020). Non-*Saccharomyces* in winemaking: Source of mannoproteins, nitrogen, enzymes, and antimicrobial compounds. *Fermentation, 6*, 76. https://doi.org/10.3390/fermentation6030076

Wenning, M., & Scherer, S. (2013). Identification of microorganisms by FTIR spectroscopy: Perspectives and limitations of the method.

Applied Microbiology and Biotechnology, 97, 7111–7120. https://doi.org/10.1007/s00253-013-5087-3

Yamaguchi, M., Namiki, Y., Okada, H., Mori, Y., Furukawa, H., Wang, J., Ohkusu, M., & Kawamoto, S. (2011). Structome of *Saccharomyces cerevisiae* determined by freeze-substitution and serial ultrathin-sectioning electron microscopy. *Journal of Electron Microscopy, 60*, 321–335. https://doi.org/10.1093/jmicro/dfr052